buildings

MDPI

Article

Study on Seismic Behavior of Cross-Shaped-Steel-Reinforced RPC Columns

Jingmin Wang [1], Zhiyu Zhu [2,*] and Kun Wang [2,*]

[1] Yangzhou Polytechnic Institute, Yangzhou 225127, China; 18805271116wjm@sina.com
[2] College of Civil Science and Engineering, Yangzhou University, Yangzhou 225127, China
* Correspondence: mx120200568@yzu.edu.cn (Z.Z.); wangkun@yzu.edu.cn (K.W.); Tel.: +86-15262292218 (Z.Z.); +86-15161443298 (K.W.)

Abstract: Based on the hysteretic tests of steel-reinforced reactive powder concrete (RPC) columns and reinforced RPC columns, the finite element numerical models of these two kinds of RPC columns were established by OpenSees (2016). The feasibility of the model was verified by comparing the results of tests and simulation. On this basis, the nonlinear analysis of seismic performance of cross-shaped-steel-reinforced RPC columns was carried out. The influences of different factors such as longitudinal reinforcement ratio, steel sectional resistance moment, RPC grade, steel strength and section form of shape steel on the hysteretic performance were investigated. Finally, the hysteretic model of cross-shaped-steel-reinforced RPC columns was established. The results showed that, compared with H-shaped-steel-reinforced RPC columns, the peak bearing capacity of cross-shaped-steel-reinforced RPC columns was increased by 21.2%, but the displacement ductility was obviously reduced. With the increase of slenderness ratio, the lateral stiffness and horizontal bearing capacity of cross-shaped steel RPC columns decreased rapidly. In addition, the peak load was improved with the increase of RPC strength, steel sectional resistance moment and longitudinal reinforcement ratio. The hysteretic model was consistent with the simulation results, which can effectively predict the hysteretic characteristics of cross-shaped-steel-reinforced RPC columns. The research results can provide a theoretical basis for the engineering design and application of cross-shaped-steel-reinforced RPC columns.

Keywords: RPC column; hysteretic performance; OpenSees; cross-shaped steel; finite element simulation

check for updates

Citation: Wang, J.; Zhu, Z.; Wang, K. Study on Seismic Behavior of Cross-Shaped-Steel-Reinforced RPC Columns. *Buildings* **2024**, *14*, 2310. https://doi.org/10.3390/buildings14082310

Academic Editor: Andreas Lampropoulos

Received: 9 May 2024
Revised: 6 July 2024
Accepted: 23 July 2024
Published: 25 July 2024

Copyright: © 2024 by the authors. Licensee MDPI, Basel, Switzerland. This article is an open access article distributed under the terms and conditions of the Creative Commons Attribution (CC BY) license (https://creativecommons.org/licenses/by/4.0/).

1. Introduction

In recent years, steel-reinforced concrete (SRC) structures have been widely used in high-rise, long-span and heavy-duty buildings. The evaluation of earthquake collapse risk of existing buildings is constantly updated [1], and new progress has been made in the internal force transmission of composite structures [2]. However, with the continuous advancement of sustainable development, the performance requirements of structure have been improved from safety to high durability, high earthquake resistance and high environmental protection [3]. In freezing and erosive environments, the low tensile properties and relatively poor durability of normal concrete (NC) lead to serious cracks or damage in SRC structures before the end of the design service life. Reactive powder concrete (RPC) is a kind of ultra-high-performance concrete (UHPC), which has ultra-high compressive strength, excellent tensile strength and durability [4,5]. When it is applied to an SRC structure to replace NC, it can not only improve the bearing capacity of the structure and reduce the cross-section size, cement consumption and carbon emissions, but also prolong the service life and reduce the maintenance cost.

At present, scholars at home and abroad have performed many tests on the seismic performance of RPC columns. Aboukifa et al. [6] conducted seismic tests on UHPC columns and found that the higher the reinforcement ratio and reinforcement grade, the better the

seismic performance of such columns. Deng et al. [7] found that the ductility and shear capacity of RPC columns were greatly affected by the axial compression ratio through finite element analysis (FEA). Qian et al. [8] carried out low-cycle cyclic loading tests on UHPC columns strengthened with glass-fiber-reinforced plastic (GFRP) bars, and found that cracks can be effectively suppressed by GFRP bars, but that the seismic performance of UHPC columns was adversely affected. He et al. [9] carried out seismic tests on high-strength steel-bar-reinforced RPC columns and found that RPC can be effectively confined by high-strength steel bars, and that the initial stiffness, ductility and bearing capacity of the specimens was improved. Abbassi et al. [10] studied the seismic performance of RPC columns strengthened with FRP based on FEA. The results showed that this kind of column had good seismic performance and ductility, and the peak load increased with the increase of RPC strength.

Furthermore, the mechanical properties of cross-shaped-steel-reinforced concrete columns have also attracted a lot of attention. Pan et al. [11] put forward a cyclic axial stress–strain model of a cross-section steel-concrete-filled steel tube and verified the accuracy of the model through test results. Jiang et al. [12] carried out a low-cycle cyclic loading test and FEA on giant cross-shaped-steel-reinforced concrete columns, and found that steel content and axial compression ratio have significant influence on the seismic performance of such columns. Nguyen et al. [13] put forward the fracture criterion of cross-shaped-steel-reinforced concrete columns based on FEA. Mostafa et al. [14] carried out seismic tests on three new types of cross-shaped-steel-reinforced high-strength lightweight aggregate concrete columns, and found that such columns demonstrate good seismic performance.

Moreover, remarkable achievements have been made in the seismic performance of steel RPC columns at home and abroad. Ji et al. [15] carried out the seismic performance test and FEA of steel-reinforced RPC columns wrapped with GFRP tubes, and put forward the hysteretic model of such columns. Ma et al. [16] carried out the low-cycle cyclic loading test on steel-reinforced UHPC columns, and the results showed that with the increase of axial compression ratio, steel-reinforced UHPC columns showed bending failure. Zhang et al. [17] investigated the influence of different parameters on the seismic performance of steel-reinforced RPC columns through tests and established the flexural capacity formula of such columns.

In practical engineering and structural design, different from H-shaped-steel-reinforced RPC columns, the influence of side webs should be considered in the calculation of the normal section bearing capacity of cross-shaped-steel-reinforced RPC columns under uniaxial eccentric compression. In addition, the vertical H-shaped steel will also affect the energy consumption and ductility of cross-shaped-steel-reinforced RPC columns. At present, there are few reports on the seismic behavior of cross-shaped-steel-reinforced RPC columns. Therefore, the numerical model of such columns will be established in this paper, and the influence of RPC grade, axial compression ratio, steel sectional resistance moment, longitudinal reinforcement ratio, stirrup ratio, slenderness ratio and section form of shape steel on seismic performance will be investigated. Finally, a horizontal load-displacement hysteretic model of cross-shaped-steel-reinforced RPC columns will be established.

2. Numerical Model of Cross-Shaped-Steel-Reinforced RPC Column

2.1. Basic Assumption

The software OpenSees (2016, University of California, Berkeley, CA, the U.S.) was used to analyze the hysteretic behavior of cross-shaped-steel-reinforced RPC columns. The basic assumptions were as follows: (1) Plane section assumption: the cross section of the member is always a plane from stress to failure, and the strain distribution is a straight line. (2) The relative slip between longitudinal reinforcement, section steel and RPC is not considered. (3) The members have sufficient shear bearing capacity. (4) Changes in stress and strain caused by temperature and humidity are not considered.

2.2. Constitutive Relationship of Materials

The Steel02 model provided by OpenSees was adopted as the constitutive relation of steel and reinforcement. The bilinear follow-up strengthening model proposed by Menegotto and Pinto [18] was adopted as the skeleton curve of Steel02, and the Bauschinger effect was considered in unloading. Figure 1 is a schematic diagram of the stress–strain (σ_s–ε_s) curve of the Steel02 model under cyclic load. In Figure 1, f_y, ε_y and E_s are yield strength, yield strain and elastic modulus, respectively.

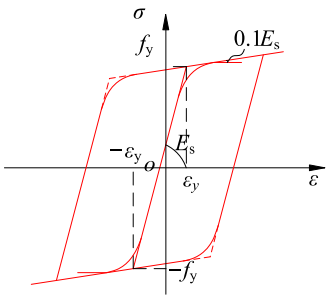


Figure 1. Steel02 model.

The Concrete07 model provided by OpenSees was adopted as stress–strain ($\sigma_c - \varepsilon_c$) curve of RPC, which is based on the Chang-Mander model [19], modified by Waugh [20]. The stress–strain relationship is shown in Figure 2, in which f_c and ε_0 are the peak axial compressive stress and strain, respectively, and f_t and ε_t are the peak axial tensile stress and strain, respectively. The calculation method can be found in reference [21]. ε^-_{cr} and ε^+_{cr} are the strains at the starting point of the straight descending branch in the compression and tension curves, respectively. ε_{sp} and ε_{crt} are the ultimate strains in compression and tension, respectively. When considering the effect of the stirrup constraint, the enhanced peak compressive stress f_{cc} and peak compressive strain ε_{cc} were calculated according to reference [22].

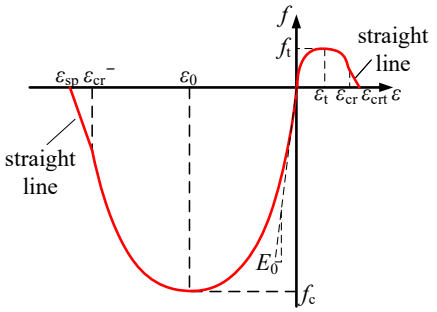


Figure 2. Concrete07 model.

2.3. Establishment of Numerical Model

As shown in Figure 3, the numerical model of cross-shaped-steel-reinforced RPC columns was established. The part from the anti-bending point to the bottom of the column was selected as the model, and the numerical model was divided into five elements along the column axis. The nonlinear beam–column element considering distributed plasticity was adopted to the elements. The division of column section is shown in Figure 3b. To consider the constraint of stirrups, the RPC section was divided into two parts: the core area and the cover concrete. The boundary condition of column bottom was fixed-bearing constraint, in which rotation and displacement in plane were not considered. The top of the column was free, and horizontal cyclic load $\pm P$ and vertical concentrated force N_0 were applied here.

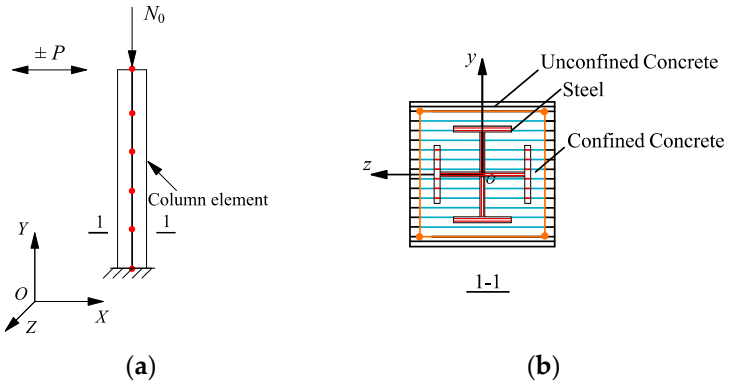


Figure 3. Numerical model of cross-shaped-steel-reinforced RPC column: (**a**) element division; (**b**) section division.

3. Verification of Numerical Model

To verify the accuracy and rationality of the above model, H-shaped-steel-reinforced RPC columns and reinforced RPC columns were selected to simulate hysteretic performance. The simulation results were compared with the test results. The simulation results can provide a basis for the effectiveness of the numerical model of the cross-shaped-steel-reinforced RPC columns.

3.1. Reinforced RPC Column

Deng et al. [7] carried out the hysteretic test of reinforced RPC columns under cyclic horizontal load. Two typical test column specimens DZ and DGZ were selected to simulate the hysteretic behavior. The size and reinforcement of the specimens are shown in Figure 4. The clear height of the column was 500 mm, and the section size was 250 mm × 250 mm. The strength grades of steel bars in specimens DZ and DGZ were HRB400 and HRB500, respectively. The measured yield strengths f_y of C10 and C16 steel bars were 472 N/mm^2 and 436 N/mm^2, respectively. The measured yield strengths f_y of D10 and D16 steel bars were 606 N/mm^2 and 551 N/mm^2, respectively. According to GB50010-2010 [23], the elastic modulus E_s of steel bars was 2.0 × 10^5 N/mm^2. The measured axial compressive and tensile strength of RPC were 120 N/mm^2 and 19.8 N/mm^2, respectively. The elastic modulus E_c was 4.32 × 10^4 N/mm^2, and the peak compressive strain ε_0 and peak tensile strain ε_t were 0.0033 and 0.0006, respectively.

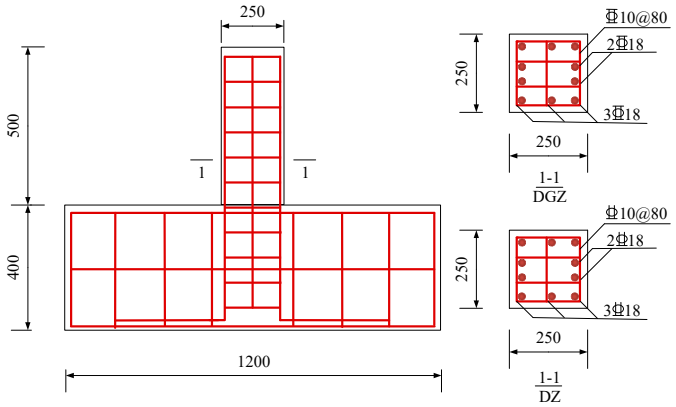


Figure 4. Specimen size and reinforcement diagram of reinforced RPC columns (size in mm).

According to the test parameters, the FEA of reinforced RPC columns was carried out by OpenSees. The constitutive relationships of RPC and steel bars were the same as those in Section 2.2. Figures 5 and 6 show the comparison of hysteretic curves and skeleton curves between test and simulation, respectively. Table 1 shows the comparison

of characteristic values of hysteretic curves between test and simulation, where + and − indicate that the loading direction is positive and negative respectively. In the table, P_m^T and P_m^C were the horizontal peak loads of test and simulation, respectively. K_y^T and K_y^C were the yield stiffness of the test and simulation, respectively. K_d^T and K_d^C were the stiffness of descending branch of the test and simulation, respectively. It can be seen that the hysteretic curves of simulation were close to the test results. The ratio P_m^T/P_m^C of peak load between test and simulation was ranging from 0.97 to 1.01, with an average value of 0.99. The ratio K_y^T/K_y^C of yield stiffness between test and simulation was between 1.02 and 1.04, with an average value of 1.03. The ratio K_d^T/K_d^C of stiffness of descending branch between test and simulation was ranging from 0.66 to 0.91, with an average of 0.79. Generally speaking, the hysteretic curves of test and simulation were in good agreement, which shows that it was feasible to simulate the hysteretic behavior of reinforced RPC columns with OpenSees software. That provided a research basis for the subsequent analysis of the hysteretic behavior of cross-shaped-steel-reinforced RPC columns.

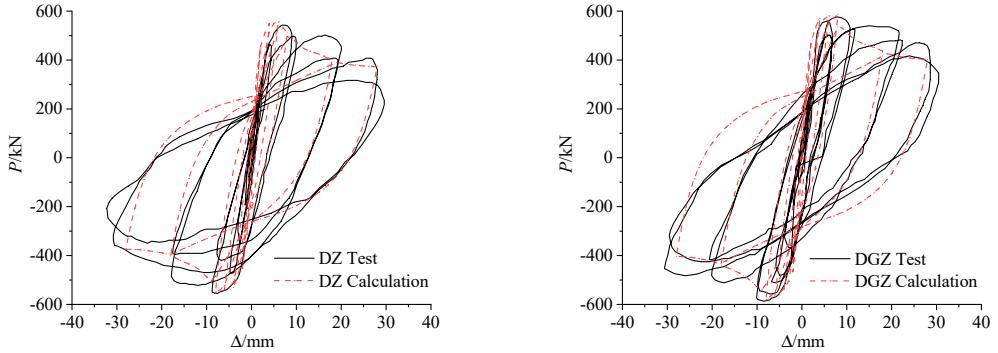


Figure 5. Comparison of test and simulation hysteretic curves: (**a**) DZ; (**b**) DGZ.

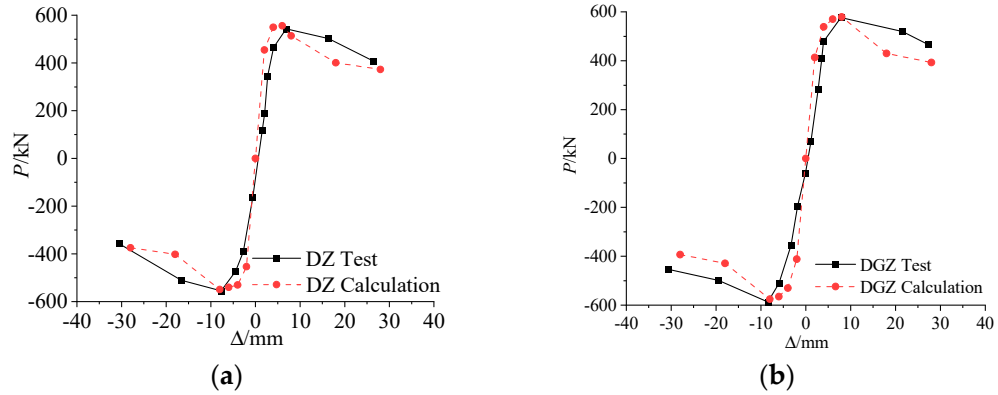


Figure 6. Comparison of test and simulation skeleton curves: (**a**) DZ; (**b**) DGZ.

Table 1. Comparison of characteristic values of test and simulated hysteretic curves.

No.	Direction	P_m^T/kN	P_m^C/kN	P_m^T/P_m^C	K_y^T /kN·mm^{-1}	K_y^C /kN·mm^{-1}	K_y^T/K_y^C	K_d^T /kN·mm^{-1}	K_d^C /kN·mm^{-1}	K_d^T/K_d^C
DZ	+	+543.09	+559.67	0.97	+6.88	+6.00	1.15	6.91	8.32	0.83
	−	−555.01	−549.26	1.01	−7.68	−8.00	0.96	8.63	8.76	0.99
DGZ	+	+577.00	+585.56	0.99	+7.84	+8.00	0.98	5.92	9.14	0.65
	−	−587.11	−581.12	1.01	−8.44	−8.00	1.06	6.01	8.88	0.68

3.2. Steel-Reinforced RPC Column

To further explore the applicability of the finite element model, the hysteretic performance of four H-shaped steel RPC columns that had been investigated in the previous research was simulated by OpenSees [17]. The test column specimens were numbered C1~C4, and the size and section reinforcement are shown in Figure 7. The clear height of the column was 1100 mm, and the distance from the bottom to the loading point was 1000 mm. Column section size was 200 mm × 200 mm. The shape steel in the column was welded with Q235 steel plates. The measured yield strengths of steel with thickness of 8 mm and 10 mm were 289 N/mm^2 and 248 N/mm^2, respectively. The elastic modulus was 2.06 × 10^5 N/mm^2 according to GB/T 228.1-2010 [24]. The longitudinal bars and stirrups were the grade of HRB400. The measured yield strengths of C8 and C18 steel bars were 463 N/mm^2 and 490.9 N/mm^2, respectively. The elastic modulus of steel bars was 2.0 × 10^5 N/mm^2 according to GB/T 228.1-2010 [24]. The measured axial compressive strength and tensile strength of RPC were 122.6 N/mm^2 and 11.0 N/mm^2, respectively. The elastic modulus was 4.3 × 10^5 N/mm^2 according to DBJ43/T 325-2017 [25]. In the simulation, the constitutive relations of RPC, shape steel and reinforcement were the same as those in Section 2.2.

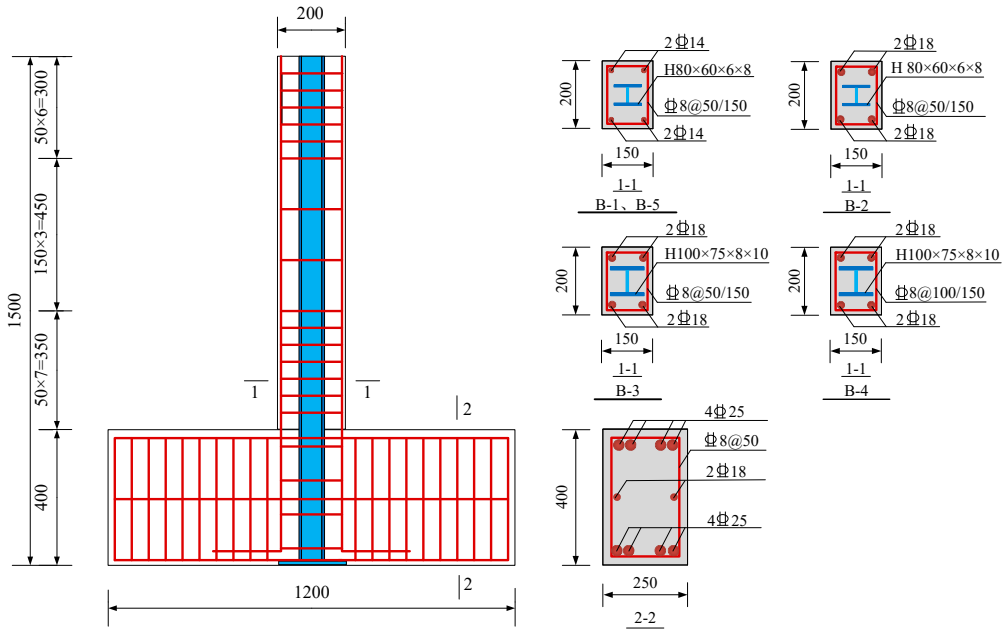


Figure 7. Specimen size and reinforcement diagram of steel-reinforced RPC columns (size in mm).

Figures 8 and 9 show the comparison of hysteretic curves and skeleton curves between the test and simulation, respectively. It can be seen that the simulation results were basically consistent with the test results. Table 2 gives a comparison of the characteristic values of the hysteretic curves between the test and simulation. It can be seen that the ratio P_m^T/P_m^C of the peak load between test and simulation was between 0.91 and 0.99, with an average value of 0.96. The ratio K_y^T/K_y^C of yield stiffness between test and simulation was ranging from 0.96 to 1.16, with an average value of 1.07. The ratio K_d^T/K_d^C of stiffness of descending branch between test and simulation was ranging from 0.89 to 1.33, with an average value of 1.16. It can be seen that the numerical model of H-shaped-steel-reinforced RPC columns established by OpenSees was feasible, which can provide a solid foundation for the analysis of hysteretic performance of cross-shaped-steel-reinforced RPC columns.

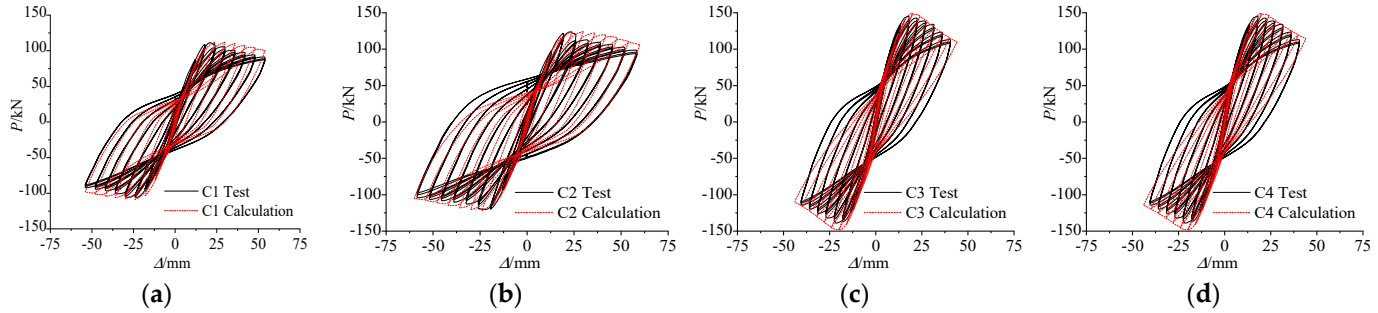


Figure 8. Comparison of test and simulation hysteretic curves: (**a**) C1; (**b**) C2; (**c**) C3; (**d**) C4.

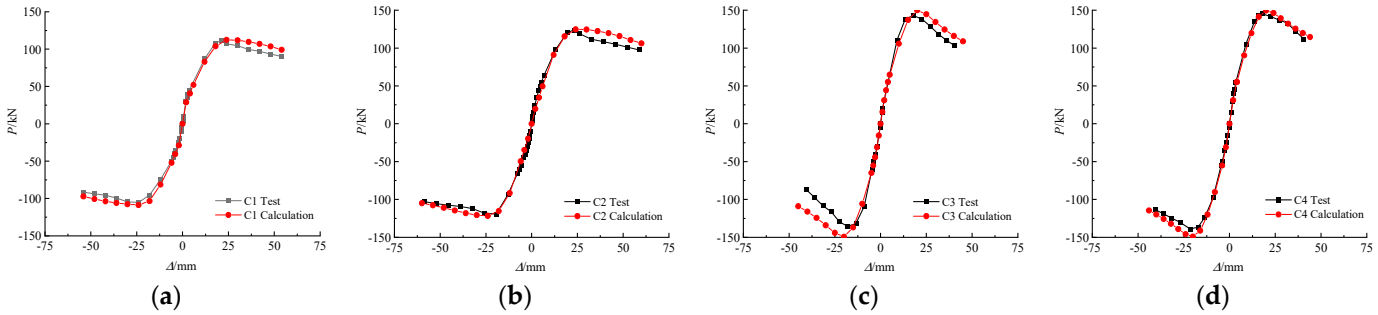


Figure 9. Comparison of test and simulated skeleton curves: (**a**) C1; (**b**) C2; (**c**) C3; (**d**) C4.

Table 2. Comparison of characteristic values of test and simulation hysteretic curves.

No.	Direction	P_m^T/kN	P_m^C/kN	P_m^T/P_m^C	K_y^T /kN·mm^{-1}	K_y^C /kN·mm^{-1}	K_y^T/K_y^C	K_d^T /kN·mm^{-1}	K_d^C /kN·mm^{-1}	K_d^T/K_d^C
C1	+	111.25	112.47	0.99	6.75	6.13	1.10	0.64	0.67	0.96
	−	−106.00	−108.83	0.97	5.41	5.61	0.96	0.46	0.36	1.28
C2	+	123.65	124.74	0.99	6.92	6.52	1.06	0.73	0.54	1.35
	−	−119.54	−121.77	0.98	6.71	6.62	1.01	0.43	0.47	0.91
C3	+	142.75	149.71	0.95	10.83	9.3	1.16	1.76	1.98	0.89
	−	−135.59	−149.1	0.91	10.55	9.3	1.13	2.15	1.62	1.33
C4	+	145.28	149.68	0.97	10.31	9.28	1.11	1.48	1.46	1.01
	−	−139.05	−149.07	0.93	9.14	9.3	0.98	1.34	1.43	0.94

4. Hysteretic Behavior of Cross-Shaped-Steel-Reinforced RPC Columns

4.1. Analysis Model

To study the seismic performance of cross-shaped-steel-reinforced RPC columns, 12 numerical specimens were established by OpenSees, numbered C-1~C-12. The cross-sectional dimensions were 250 mm× 250 mm. The main investigation factors were section form of shape steel (cross-shaped steel and H-shaped steel), axial compression ratio, RPC strength, section resistance distance of shape steel, reinforcement ratio, stirrup ratio and slenderness ratio. Table 3 gives the main parameters of the specimens. The strength of shape steel was 355 MPa, and the strength of longitudinal bars and stirrups was 400 MPa. The axial compressive and tensile strength of RPC were calculated according to reference [21].

Table 3. Main parameters of specimens.

No.	Shape Steel Size/mm	Section Resistance Distance W_{ss}/cm^3	Longitudinal Bar	Reinforcement Ratio ρ/%	RPC Strength Grade /MPa	Axial Compression Ratio n_0	Stirrup	Volume Stirrup Ratio ρ_{sv}/%	Column Length l /m	Slenderness Ratio
C-1	2 × H150 × 75 × 5 × 7	86.1	4Φ18	1.63%	C120	0.6	Φ8@80	1.26	1.2	9.6
C-2	2 × H150 × 75 × 5 × 7	86.1	4Φ18	1.63%	C120	0.4	Φ8@80	1.26	1.2	9.6
C-3	2 × H150 × 75 × 5 × 7	86.1	4Φ18	1.63%	C120	0.2	Φ8@80	1.26	1.2	9.6
C-4	2 × H150 × 75 × 5 × 7	86.1	4Φ18	1.63%	C140	0.2	Φ8@80	1.26	1.2	9.6
C-5	2 × H150 × 75 × 5 × 7	86.1	4Φ18	1.63%	C160	0.2	Φ8@80	1.26	1.2	9.6
C-6	2 × H150 × 75 × 5 × 7	86.1	4Φ22	2.43%	C120	0.2	Φ8@80	1.26	1.2	9.6
C-7	2 × H175 × 90 × 5 × 8	134.2	4Φ22	2.43%	C120	0.2	Φ8@80	1.26	1.2	9.6
C-8	2 × H150 × 75 × 5 × 7	86.1	4Φ22	2.43%	C120	0.2	Φ8@150	0.67	1.2	9.6
C-9	2 × H150 × 75 × 5 × 7	86.1	4Φ22	2.43%	C120	0.2	Φ10@80	1.96	1.2	9.6
C-10	2 × H150 × 75 × 5 × 7	86.1	4Φ18	1.63%	C120	0.4	Φ8@80	1.26	0.8	6.4
C-11	2 × H150 × 75 × 5 × 7	86.1	4Φ18	1.63%	C120	0.4	Φ8@80	1.26	1.6	12.8
C-12	1 × H150 × 75 × 5 × 7	86.1	4Φ18	1.63%	C120	0.2	Φ8@80	1.26	1.2	9.6

4.2. Hysteretic Curve

Figure 10 shows the hysteretic curves of the 12 specimens. It can be seen that: (1) At the initial stage of loading, the area of the hysteretic curve was small, and it can return to the original point when unloading, indicating that the specimens were in the elastic stage. (2) With the increase of displacement, the area of hysteretic curve gradually increased, the slope of the curve gradually decreased and the residual deformation became larger. At this point, the specimens were in the elastic-plastic stage. (3) After the peak load was reached, the bearing capacity of the specimens began to decrease and the horizontal displacement changed quickly. After unloading, the residual deformation continued to increase.

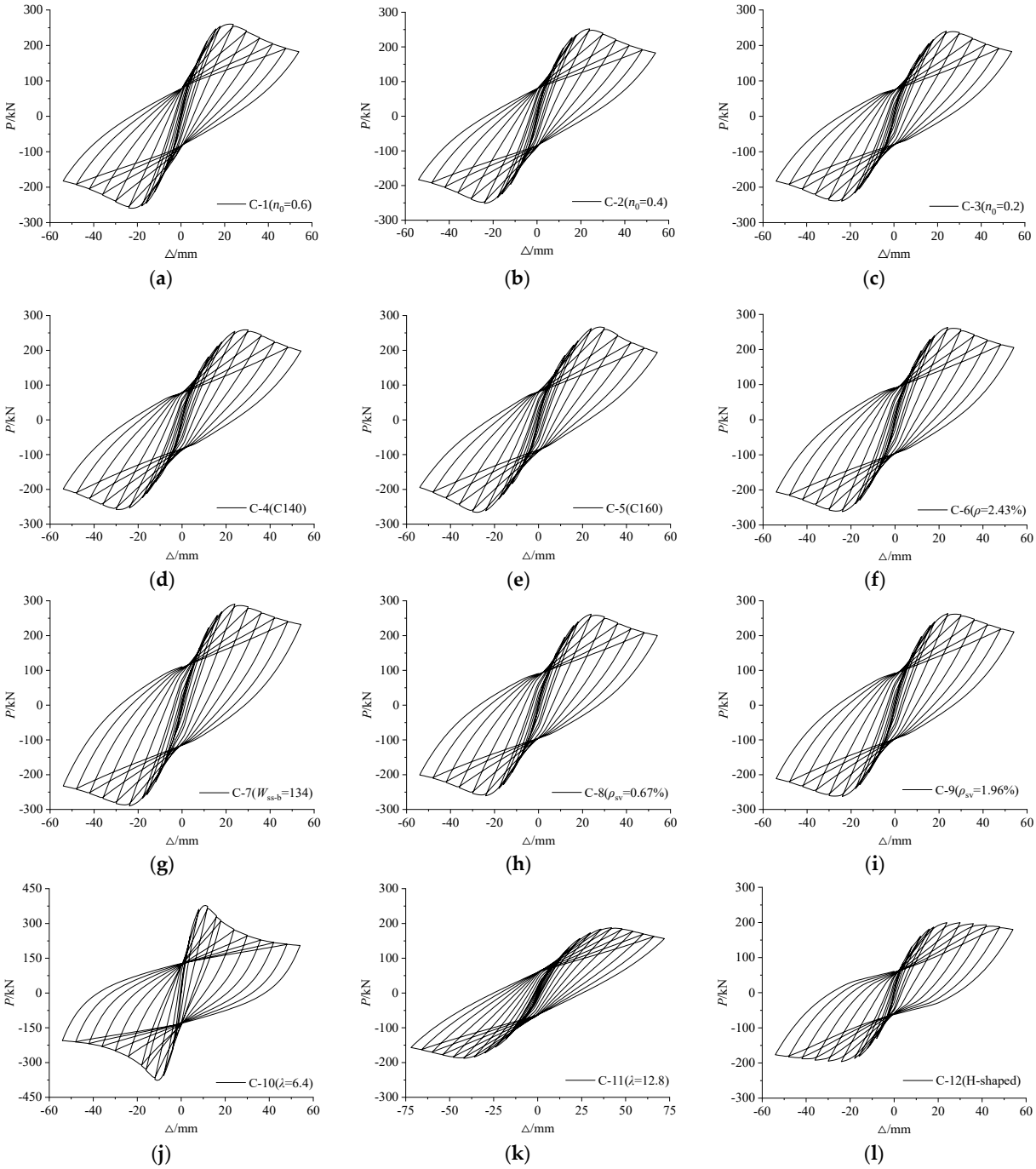


Figure 10. Hysteretic curve: (**a**) C-1; (**b**) C-2; (**c**) C-3; (**d**) C-4; (**e**) C-5; (**f**) C-6; (**g**) C-7; (**h**) C-8; (**i**) C-9; (**j**) C-10; (**k**) C-11; (**l**) C-12.

4.3. Skeleton Curve

The skeleton curves of the 12 specimens are shown in Figure 11, and the influences of different parameters are as follows: (1) As shown in Figure 11a, with the increase of axial compression ratio, the peak load increased, the displacement corresponding to the peak load decreased and the descending branch after the peak load became steeper. (2) As can be seen from Figure 11b, when the RPC strength was less than 140 MPa, with the increase of RPC strength, the initial stiffness and peak load of the specimen increased. However, when the RPC strength was higher than 140 MPa, the improvement of RPC strength had little effect on the seismic performance of the specimens. (3) As can be seen from Figure 11c, with the increase of reinforcement ratio and steel sectional resistance moment, the initial stiffness and peak load of the specimen was increased obviously, and the skeleton curve shape was similar. (4) From Figure 11d, it can be seen that the increase of volume stirrup ratio had little effect on the peak load, but it could improve the stiffness of the descending branch. (5) As can be seen from Figure 11e, with the increase of slenderness ratio of the specimen, the initial stiffness and peak bearing capacity of the specimens were obviously reduced, but the slope of the descending branch became gentle. (6) As can be seen from Figure 11f, compared with the H-shaped steel RPC column, the peak load of the cross-shaped-steel-reinforced RPC column was increased by 21.20%. But the descending branch of the cross-shaped-steel-reinforced RPC column was steeper, which indicated that the ductility was reduced to some extent.

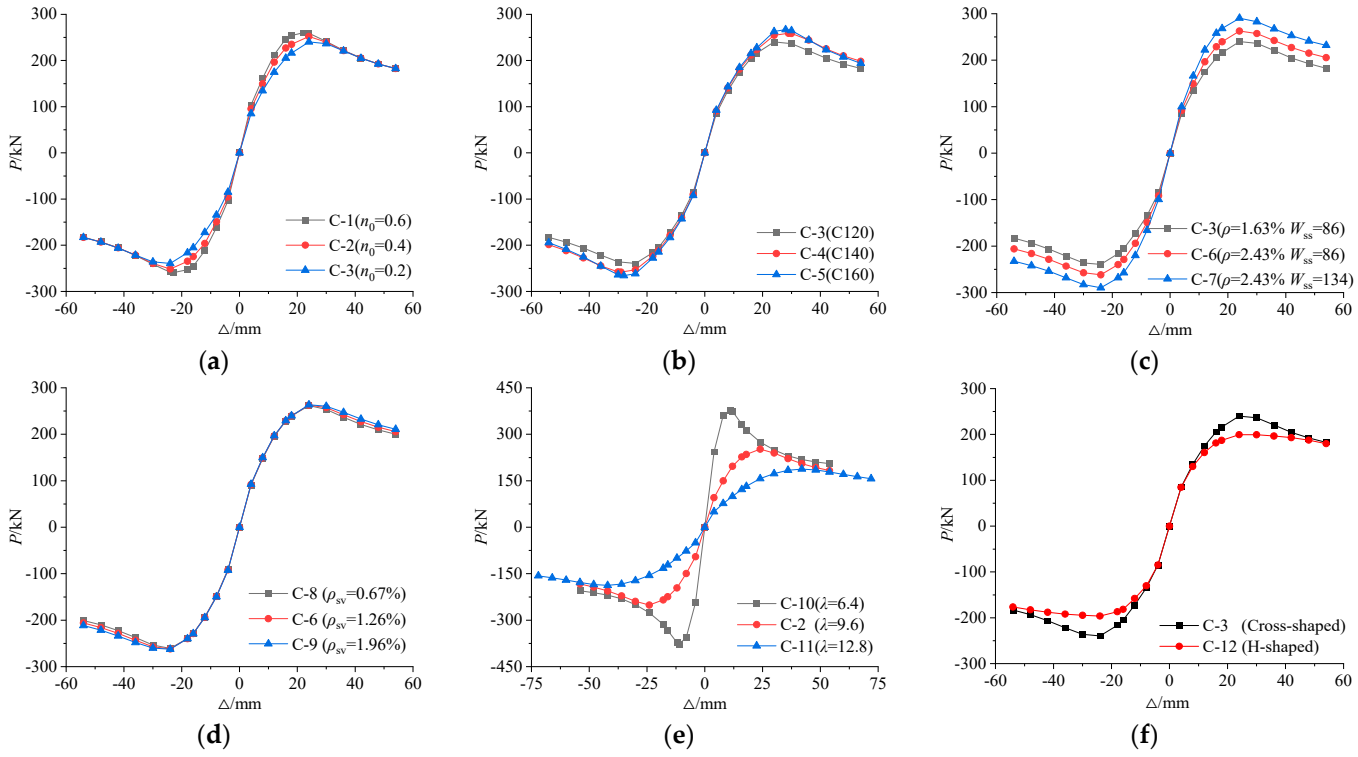


Figure 11. Skeleton curve: (**a**) axial compression ratio; (**b**) RPC strength; (**c**) reinforcement ratio and steel sectional resistance moment; (**d**) stirrup ratio; (**e**) slenderness ratio; (**f**) configuration form of steel.

4.4. Displacement Ductility

The yield point was determined by energy equivalence method [26]. Table 4 gives the yield strength P_y, yield displacement Δ_y, peak load P_m, displacement ductility coefficient u and other characteristic values of the specimens. It can be seen that the ductility increased with the increase of axial compression ratio, reinforcement ratio, stirrup ratio and slenderness ratio. However, with the increase of RPC strength and steel sectional

resistance moment, the ductility decreased obviously. The ductility of the specimen with H-shaped steel was obviously larger than that of the specimen with cross-shaped steel, and the average ductility had increased from 2.65 to 4.54, which is an improvement of about 71%.

Table 4. Displacement ductility.

No.	Direction	P_y /kN	Δ_y /mm	P_m /kN	Δ_u /mm	μ	No.	Direction	P_y /kN	Δ_y /mm	P_m /kN	Δ_u /mm	μ
C-1	+	227.45	13.74	260.15	36.30	2.64	C-7	+	256.81	15.84	290.50	45.07	2.85
	–	226.79	13.76	259.36	36.59	2.66		–	255.96	15.85	289.70	45.91	2.90
C-2	+	220.30	15.12	251.96	38.64	2.56	C-8	+	229.50	16.14	261.63	41.58	2.58
	–	218.49	15.14	251.37	39.00	2.58		–	229.43	16.14	260.84	42.38	2.63
C-3	+	208.05	16.53	240.01	42.37	2.56	C-9	+	230.00	16.15	263.36	46.39	2.87
	–	208.23	16.53	239.31	43.31	2.62		–	229.78	16.15	262.54	47.27	2.93
C-4	+	221.47	17.65	258.98	44.02	2.49	C-10	+	336.10	7.14	377.86	17.18	2.41
	–	221.54	17.66	258.11	45.12	2.56		–	333.76	7.21	376.61	17.35	2.41
C-5	+	227.00	17.91	266.90	40.97	2.29	C-11	+	162.17	25.98	187.67	69.29	2.67
	–	226.79	17.87	265.91	41.82	2.34		–	161.38	26.10	187.60	69.60	2.67
C-6	+	229.92	16.16	262.8	43.88	2.72	C-12	+	170.84	13.99	199.44	61.87	4.42
	–	229.79	16.16	261.99	44.78	2.77		–	167.40	13.63	196.04	63.47	4.65

4.5. Stiffness Degradation

The stiffness degradation of the specimen is taken as secant stiffness, and the secant stiffness K_i under each cyclic load is calculated according to Formula (1), where F_i and X_i are the i-th peak point load and displacement, respectively.

$$K_i = \frac{|+F_i| + |-F_i|}{|+X_i| + |-X_i|} \quad (1)$$

Figure 12 shows the stiffness degradation curves of 12 simulated specimens. As can be seen from Figure 12a, before reaching the peak load, the secant stiffness of the specimen increased with the increase of axial compression ratio. After reaching the peak load, with the increase of displacement, the secant stiffness of specimens tended to be consistent. It can be seen from Figure 12b that the secant stiffness increased with the increase of RPC strength before RPC strength reached 140 MPa, but when RPC strength was higher than 140 MPa, the increase of RPC strength had little effect on secant stiffness. As can be seen from Figure 12c, the secant stiffness increased with the increase of reinforcement ratio and sectional resistance moment, and the degradation trend was basically the same. It can be seen from Figure 12d that the stiffness degradation curves under different volume stirrup ratios were close, which indicated that the change of volume stirrup ratio had little effect on the stiffness degradation. As can be seen from Figure 12e, with the increase of slenderness ratio, the initial secant stiffness and stiffness degradation rate of the specimen decreased obviously. At the later stage of loading, the secant stiffness of the specimens tended to be the same. As can be seen from Figure 12f, the secant stiffness of the specimen with cross-shaped steel and the specimen with H-shaped steel were not much different at the initial stage of loading. With the increase of displacement, the secant stiffness of the specimen with cross-shaped steel was greater than that of the specimen with H-shaped. At the later stage of loading, the secant stiffness of the two specimens was basically the same.

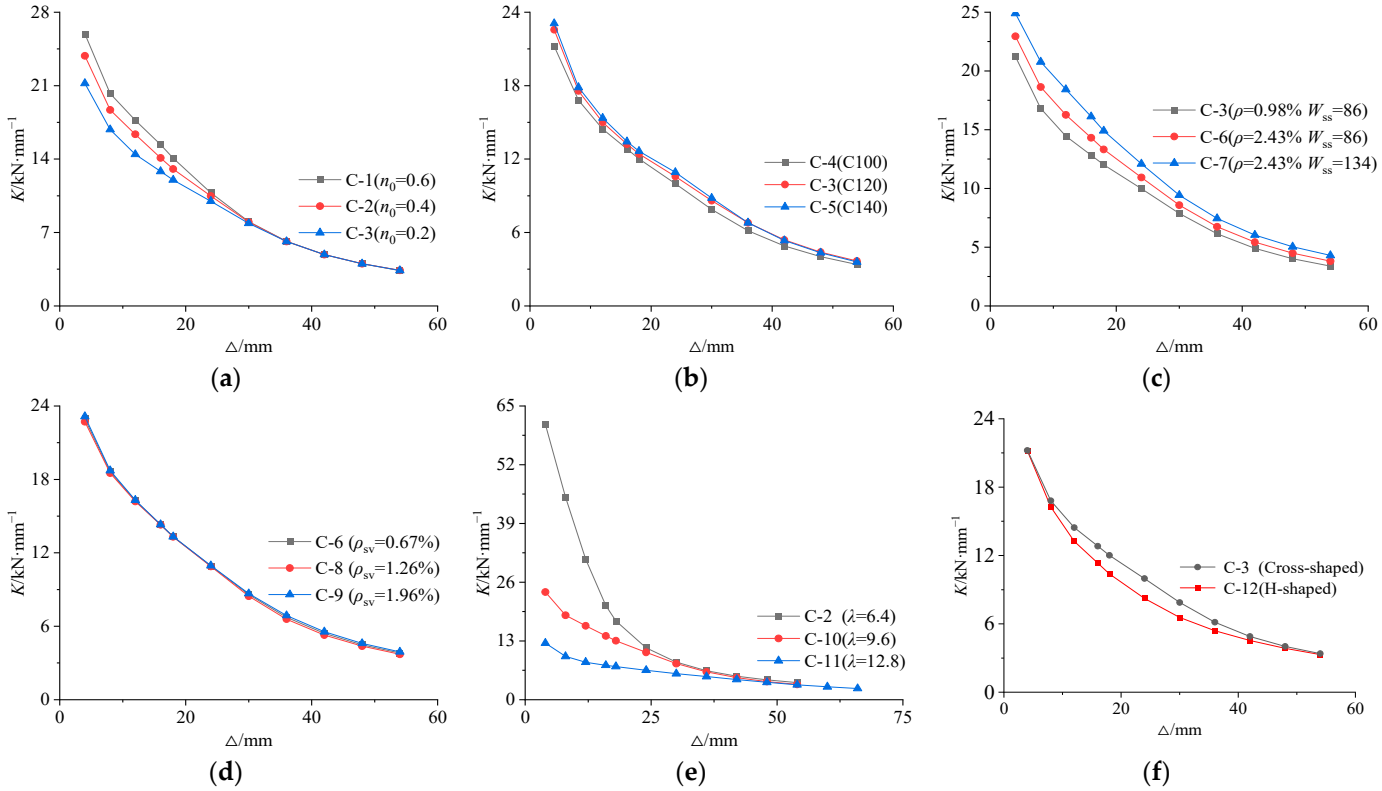


Figure 12. Stiffness degradation: (**a**) axial compression ratio; (**b**) RPC strength; (**c**) reinforcement ratio and steel sectional resistance moment; (**d**) stirrup ratio; (**e**) slenderness ratio; (**f**) configuration form of steel.

4.6. Energy Dissipation Capacity

In this paper, the energy dissipation coefficient E was used to measure the energy dissipation capacity of the specimens. The energy dissipation coefficient is calculated according to Formula (2), where S_{ABCDE} is the area of hysteresis loop of the specimen, and S_{OBF} and S_{ODG} are the areas of the triangle corresponding to the upper and lower vertices of the hysteretic loop, as shown in Figure 13.

$$E = \frac{S_{ABCDE}}{S_{OBF} + S_{ODG}} \tag{2}$$

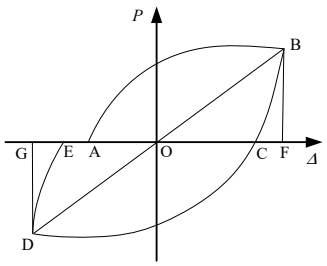


Figure 13. Schematic diagram of viscous damping coefficient calculation.

The energy dissipation coefficients of the 12 specimens are shown in Figure 14. It can be seen as follows: (1) Comparing the specimens C-1~C-3, with the increase of axial compression ratio, the energy dissipation capacity of the specimens was improved in the middle stage of loading, but the total energy dissipation capacity was basically the same. (2) Comparing the specimens C-3~C-5, the energy dissipation capacity decreased with the increase of RPC strength, which may be due to the increase of initial stiffness. (3) As

can be seen from Figure 14c, with the increase of reinforcement ratio and steel sectional resistance moment, the energy dissipation capacity increased obviously. (4) Comparing the specimens C-6, C-8 and C-9, the increase of volume stirrup ratio has little effect on the energy dissipation capacity of the specimens. (5) As can be seen from Figure 14e, with the increase of the slenderness ratio of the specimens, the energy dissipation capacity of the specimens under each displacement was obviously reduced, and the total energy dissipation was also obviously reduced. (6) Comparing the specimens C-3 and C-12, it can be seen that the total energy dissipation capacity of the specimen with cross-shaped steel was better than that of the specimen with H-shaped steel.

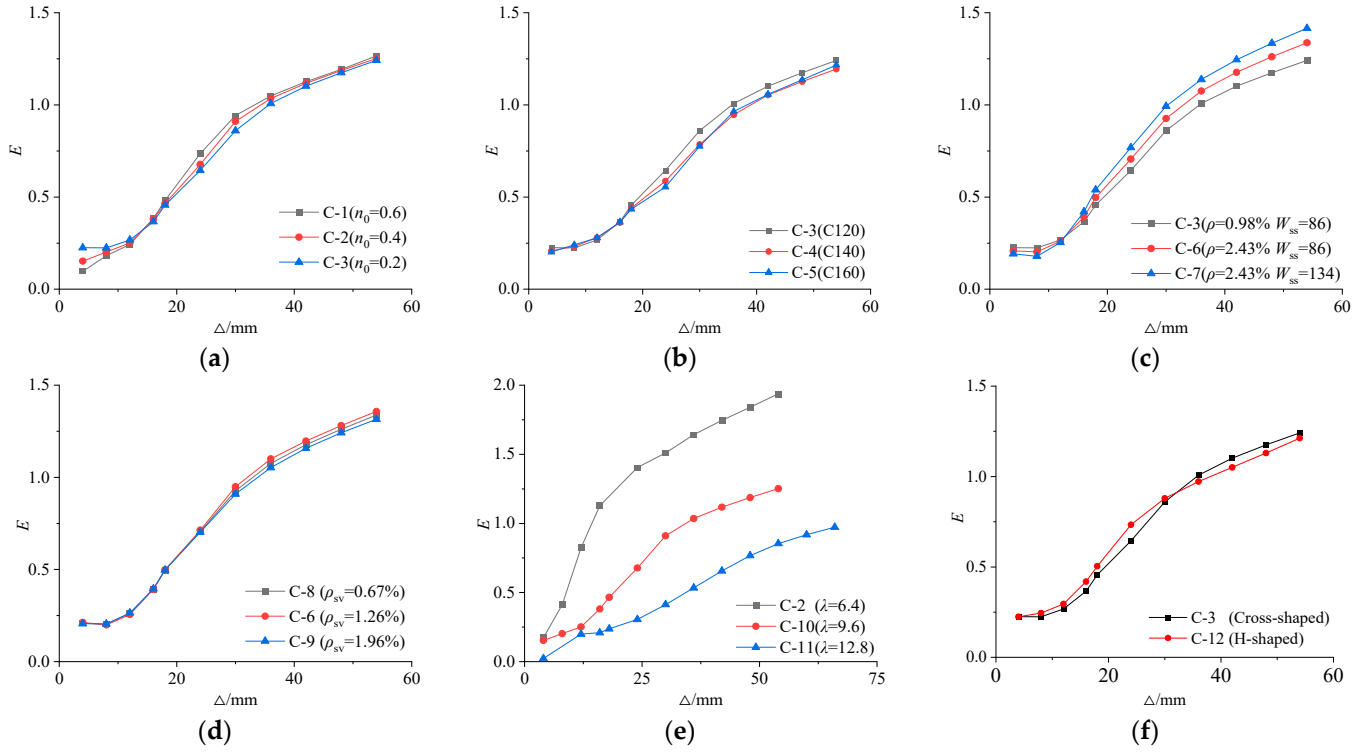


Figure 14. Energy dissipation coefficient: (**a**) axial compression ratio; (**b**) RPC strength; (**c**) reinforcement ratio and steel sectional resistance moment; (**d**) stirrup ratio; (**e**) slenderness ratio; (**f**) configuration form of steel.

5. Hysteretic Model

5.1. Skeleton Curve

The degenerate trilinear model was adopted as the skeleton curve model. It is necessary to determine three characteristic points: yield point *Y*, peak point *M* and failure point *U*, as shown in Figure 15a. According to the results of numerical regression, the yield stiffness K_y and yield load P_y of cross-shaped-steel-reinforced RPC columns can be calculated according to Formulas (3) and (4), respectively. The stiffness of descending branch can be calculated according to Formula (5), where E_aI_a and E_cI_c are the stiffness of shape steel and RPC, respectively. l is the length of column and n_0 is the axial compression ratio.

$$K_y = 3\left[E_aI_a + \left(0.44 + 0.3646n_0^2\right)E_cI_c\right]/l^3 \quad (3)$$

$$P_y = \left(-0.052n_0^2 + 0.054n_0 + 0.86\right)P_m \quad (4)$$

$$K_d = \left(-0.334n_0^2 + 0.289n_0 + 0.116\right)K_y \quad (5)$$

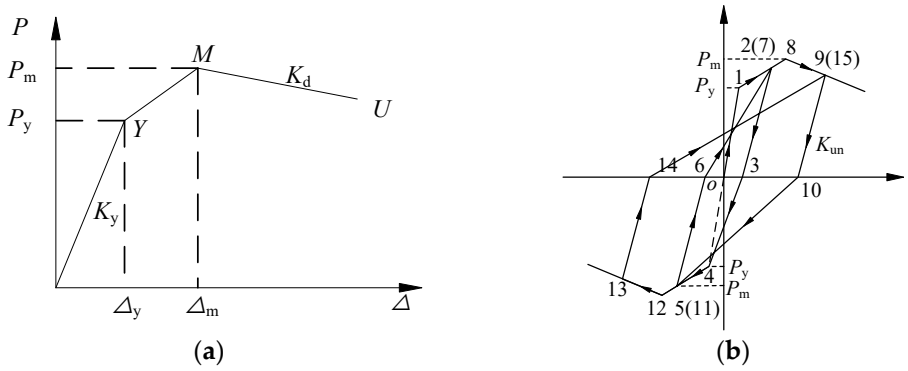


Figure 15. Hysteretic model: (**a**) skeleton curve; (**b**) hysteresis rule.

5.2. Hysteresis Rule

Figure 15b shows the hysteretic rule of cross-shaped-steel-reinforced RPC columns. The numbers from small to large indicate the walking route of the model in the process of forward and backward loading and unloading. The specific hysteretic rules are as follows: (1) Before the horizontal load reaches yield load P_y, there is no stiffness degradation or residual deformation, and the specimen is loaded and unloaded according to the walking route of 0–1 and 1–0, respectively. (2) When the restoring force is between the P_y and the peak load P_m, the incremental stiffness of the specimen after yield is taken as loading stiffness. The unloading stiffness K_{un} is the reduction of the initial stiffness, which is calculated according to Formula (6), where Δ_{un} is the maximum displacement experienced. (3) When the restoring force exceeds the peak load P_m, the stiffness K_d is used as the loading stiffness. The unloading stiffness continues to be determined according to Formula (6). (4) When the specimen is subjected to backward load, if the yield load is not exceeded, the path follows from $P = 0$ to the yield load P_y. Once the load exceeds the yield load, the path moves from $P = 0$ to the maximum load point ever passed in the backward direction. When forward reloading after backward unloading, the path goes directly from $P = 0$ to the maximum load point ever passed in the forward direction.

$$K_{un} = 1.291\left(\frac{\Delta_{un}}{\Delta_y}\right)^{-0.7515} K_y \tag{6}$$

5.3. Comparison between Simulated Hysteretic Curve and Hysteretic Model

The 12 cross-shaped-steel-reinforced RPC specimens were predicted by the above hysteretic model. The comparison between the hysteretic curves predicted by hysteretic model and that calculated by numerical simulation is shown in Figure 16. It can be found that the two results are in good agreement, which shows that the hysteretic model established in this paper is reliable.

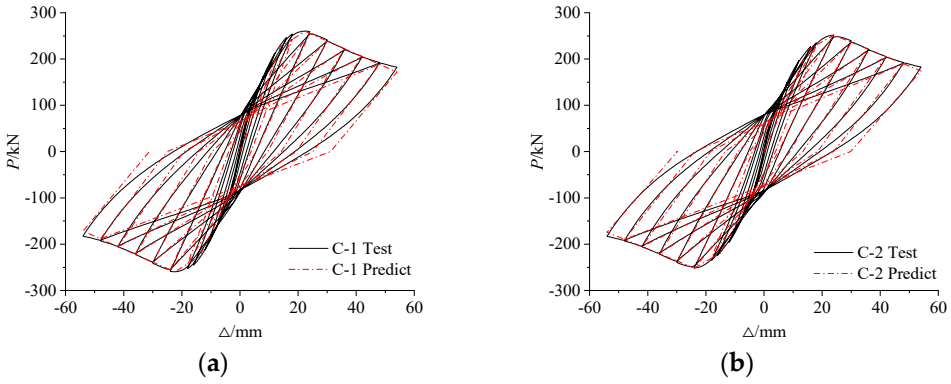


Figure 16. *Cont.*

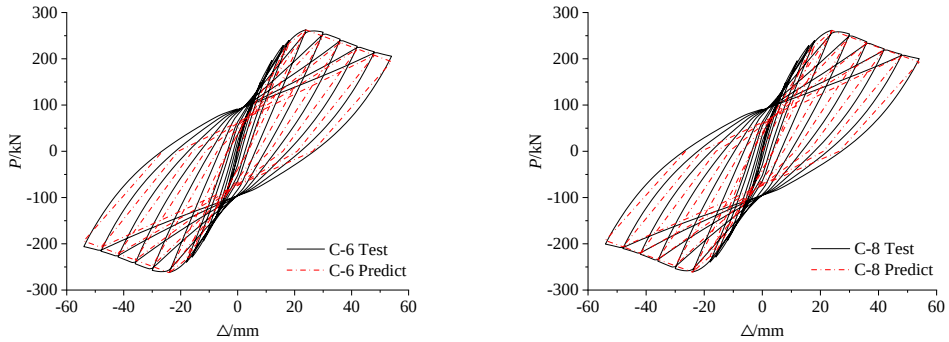


Figure 16. Comparison between hysteretic model and simulated hysteretic curve: (**a**) C-1; (**b**) C-2; (**c**) C-6; (**d**) C-8.

6. Discussion

This study was mainly based on the existing literature; after establishing the finite element model and verifying its feasibility and rationality, the nonlinear parameter analysis was carried out. The research results are reliable to some extent, but related tests are still needed.

7. Conclusions

Based on the nonlinear beam–column element, the numerical model of cross-shaped-steel-reinforced RPC columns was established by OpenSees. The hysteretic behavior of such columns under horizontal cyclic load was studied, and the following conclusions are drawn:

(1) The calculated results of the models of reinforced RPC columns and steel-reinforced RPC columns were in good agreement with the test results. The average difference of peak load, yield stiffness and stiffness of descending branch was 2.75%, 5.50% and 1.5%, respectively. It shows that the established numerical model had high reliability and can provide theoretical support for subsequent parameter analysis.

(2) The results of hysteretic analysis show that the cross-shaped-steel-reinforced RPC column had good seismic performance. Steel sectional resistance moment and reinforcement ratio were two important factors that affected the hysteretic behavior of cross-shaped-steel-reinforced RPC columns. With the increase of steel sectional resistance moment and reinforcement ratio, the peak load and energy dissipation capacity were significantly improved, but it has little effect on ductility.

(3) Compared with H-shaped-steel-reinforced RPC columns, the peak bearing capacity of cross-shaped-steel-reinforced RPC columns was increased by 21.2%, but the ductility decreased. The total energy dissipation capacity of the specimen with cross-shaped steel was better than that of the specimen with H-shaped steel.

(4) According to the results of parametric analysis, the hysteretic model of cross-shaped-steel-reinforced RPC columns was established. The hysteretic curves predicted by the hysteretic model were basically consistent with the numerical analysis results. The hysteretic model provides a theoretical basis for the hysteretic analysis of cross-shaped-steel-reinforced RPC columns.

(5) For cross-shaped steel columns, RPC with 140 MPa is an economical choice. In this case, the axial compression ratio and slenderness ratio can be reasonably improved according to the use of the building. Cross-shaped steel columns are recommended in disaster-prone areas where the direction of earthquake load cannot be predicted, because when the earthquake load is perpendicular to the web of the H-beam, its seismic performance will be difficult to give full play.

(6) The conclusions were summarized according to the results of parameter analysis, which was based on the numerical model established by the existing literature. The

conclusions are reliable to some extent, but related tests are still needed for further verification.

Author Contributions: Conceptualization, J.W.; data curation, K.W.; investigation, J.W.; methodology, J.W.; software, Z.Z.; validation, Z.Z.; visualization, K.W.; writing—original draft, Z.Z.; writing—review and editing, K.W. All authors have read and agreed to the published version of the manuscript.

Funding: This research was funded by the National Natural Science Foundation of China (51878589) and the Open Fund of Key Lab of Structures Dynamic Behavior and Control of the Ministry of Education (HITCE202105).

Data Availability Statement: The original contributions presented in the study are included in the article, further inquiries can be directed to the corresponding authors.

Acknowledgments: The authors gratefully acknowledge the support provided by the National Natural Science Foundation of China (51878589) and the Open Fund of Key Lab of Structures Dynamic Behavior and Control of the Ministry of Education (HITCE202105).

Conflicts of Interest: The authors declare no conflicts of interest.

References

1. Tsiavos, A.; Amrein, P.; Bender, N.; Stojadinovic, B. Compliance-based estimation of seismic collapse risk of an existing reinforced concrete frame building. *Bull. Earthq. Eng.* **2021**, *19*, 6027–6048. [CrossRef]
2. Vigneri, V.; Kroyer, R.; China, S.; Argentoni, A.; Taras, A. Longitudinal Shear Transfer in Composite Steel Truss and Concrete (CSTC) BEAMS. *ce/Papers* **2023**, *6*, 682–693. [CrossRef]
3. Jonnalagadda, S.; Chava, S. Ultra-High-Performance Concrete (UHPC): A state-of-the-art review of material behavior, structural applications and future. *Electron. J. Struct. Eng.* **2023**, *23*, 25–30. [CrossRef]
4. Saladi, N.; Montanari, L.; De la Varga, I.; Spragg, R.; Graybeal, B. Assessing durability properties of ultra-high performance concrete-class materials. *Mater. Struct.* **2023**, *56*, 155. [CrossRef]
5. Kusumawardaningsih, Y.; Fehling, E.; Ismail, M.; Aboubakr, A.A.M. Tensile strength behavior of UHPC and UHPFRC. *Procedia Eng.* **2015**, *125*, 1081–1086. [CrossRef]
6. Aboukifa, M.; Moustafa, M.A. Experimental seismic behavior of ultra-high performance concrete columns with high strength steel reinforcement. *Eng. Struct.* **2021**, *232*, 111885. [CrossRef]
7. Deng, Z.; Gu, J.; He, S. Numerical simulation on seismic performance of reactive powder concrete short columns. *Build. Sci.* **2019**, *35*, 119–127. (In Chinese)
8. Qian, K.; Xue, T.-Q.; Deng, X.-F.; Ma, J. Experimental investigation on seismic behavior of Ultra-high performance concrete columns reinforced with GFRP bars. *Structures* **2023**, *53*, 568–580. [CrossRef]
9. He, S.; Deng, Z.; Yao, J. Seismic behavior of ultra-high performance concrete long columns reinforced with high-strength steel. *J. Build. Eng.* **2020**, *32*, 101740. [CrossRef]
10. Abbassi, M.; Dabbagh, H. Seismic response of reactive powder concrete columns confined with FRP. *Slovak J. Civil Eng.* **2019**, *27*, 12–20. [CrossRef]
11. Pan, M.; Wang, D. Cyclic axial compression stress-strain model for FRP-confined concrete-encased cross-shaped steel columns. *Eng. Struct.* **2024**, *298*, 117063. [CrossRef]
12. Jiang, H.; Li, Y.; Zhu, J. Numerical simulation of mega steel reinforced concrete columns with different steel sections. *Struct. Des. Tall Spec. Build.* **2017**, *26*, e1304. [CrossRef]
13. Nguyen, D.H.; Hong, W.K. Part I: Failure criteria of the steel-concrete columns (SRC columns) confined by cross-shaped flange sections. *J. Asian Archit. Build. Eng.* **2021**, *20*, 179–192. [CrossRef]
14. Mostafa, M.M.; Chen, S.; Wu, T.; Liu, X.; Liu, Y. Experimental seismic analysis of new types of steel-reinforced lightweight concrete columns with cross-shaped steel section. *J. Build. Eng.* **2022**, *60*, 105202. [CrossRef]
15. Ji, J.; He, L.; Jiang, L.; Ren, H.; Ni, S.; Wang, Z.; Li, Y.; Yu, C.; Lin, Y. Seismic behavior of GFRP tube reactive powder concrete composite columns with encased steel. *Front. Mater.* **2021**, *8*, 793392. [CrossRef]
16. Ma, Y.; Jia, J.; Zhu, W. Comparative analysis of the seismic behaviour of SRUHSC columns and frames under reverse cyclic loading. *Mag. Concr. Res.* **2018**, *70*, 189–203. [CrossRef]
17. Zhang, L.; Wang, K.; Zhang, M.; Yang, Y.; Liu, F.; Yang, D.; Xu, G.; Chen, W. Seismic performance of steel-reinforced reactive powder concrete columns. *Structures* **2023**, *54*, 1788–1802. [CrossRef]
18. Menegotto, M.; Pinto, P.E. Method of Analysis for Cyclically Loaded Reinforced Concrete Plane Frames including Changes in Geometry and Non-elastic Behavior of Elements under Combined Normal Force and Bending. In Proceedings of the IABSE Symposium on Resistance and Ultimate Deformability of Structures Acted on by Well Defined Repeated Loads, Lisbon, Portugal, September 1973.

19. Chang, G.A.; Mander, J.B. *Seismic Energy Based Fatigue Damage Analysis of Bridge Columns: Part 1—Evaluation of Seismic Capacity*; State University of New York: New York, NY, USA, 1994.
20. Waugh, J.D. *Nonlinear Analysis of T-Shaped Concrete Walls Subjected to Multi-Directional Displacements*; Iowa State University: Ames, IA, USA, 2009.
21. Lv, X.; Wang, Y.; Fu, C. Basic mechanical property indexes of reactive powder concrete. *J. Harbin Inst. Technol.* **2014**, *46*, 9. (In Chinese)
22. Deng, Z.; Yao, J. The axial compression stress-strain model for ultra-high performance concrete columns confined by high-strength stirrups. *Eng. Mech.* **2020**, *37*, 120–128. (In Chinese)
23. *GB 50010-2010*; Code for Design of Concrete Structures. China Building Industry Press: Beijing, China, 2010. (In Chinese)
24. *GB/T 228.1-2010*; Tensile Test Method of Metallic Materials at Room Temperature. China Standards Publishing House: Beijing, China, 2010. (In Chinese)
25. *DBJ 43/T 325-2017*; Technical Specification for Reactive Powder Concrete Structure. China Building Industry Press: Beijing, China, 2017. (In Chinese)
26. Xue, J.; Zhang, X.; Ke, X.; Ma, L. Seismic resistance capacity of steel reinforced highstrength concrete columns with rectangular spiral stirrups. *Constr. Build. Mater.* **2019**, *229*, 116880. [CrossRef]

Disclaimer/Publisher's Note: The statements, opinions and data contained in all publications are solely those of the individual author(s) and contributor(s) and not of MDPI and/or the editor(s). MDPI and/or the editor(s) disclaim responsibility for any injury to people or property resulting from any ideas, methods, instructions or products referred to in the content.